Journal of
Composites Science

MDPI

Article

Impact Resistance Enhancement of Sustainable Geopolymer Composites Using High Volume Tile Ceramic Wastes

Ghasan Fahim Huseien [1,*], Ziyad Kubba [2], Akram M. Mhaya [3], Noshaba Hassan Malik [4] and Jahangir Mirza [5]

1 Department of the Built Environment, College of Design and Engineering, National University of Singapore, Lower Kent Ridge, Singapore 117566, Singapore
2 Department of Civil Engineering, College of Engineering, Al-Muthanna University, Samawa 66001, Iraq
3 Faculty of Civil Engineering and Built Environment, Universiti Tun Hussein Onn Malaysia, Parit Raja 86400, Johor, Malaysia
4 Department of Botany, Rawalpindi Women University, Rawalpindi 46300, Pakistan
5 Department of Civil Engineering, York University, Toronto, ON M4N 3M6, Canada
* Correspondence: bdggfh@nus.edu.sg; Tel.: +65-83057143

Abstract: The need for sustainable concrete with low carbon dioxide emissions and exceptional performance has recently increased in the building industry. Many distinct types of industrial byproducts and ecologically safe wastes have shown promise as ingredients for this kind of concrete. Meanwhile, as industrialization and lifestyle modernization continue to rise, ceramic waste becomes an increasingly serious threat to the natural environment. It is well known that free cement binder that incorporates tile ceramic wastes (TCWs) can significantly improve the material's sustainability. We used this information to create a variety of geopolymer mortars by mixing TCWs with varied proportions of ground blast furnace slag (GBFS) and fly ash (FA). Analytical techniques were used to evaluate the mechanical properties and impact resistance (IR) of each designed mixture. TCWs were substituted for binders at percentages between 50 and 70 percent, and the resultant mixes were strong enough for real-world usage. Evidence suggests that the IR and ductility of the proposed mortars might be greatly improved by the addition of TCWs to a geopolymer matrix. It was found that there is a trend for both initial and failure impact energy to increase with increasing TCWs and FA content in the matrix. The results show that the raising of TCWs from 0% to 50, 60 and 70% significantly led to an increase in the failure impact energy from 397.3 J to 456.8, 496.6 and 595.9 J, respectively.

Keywords: geopolymer composites; tile ceramic wastes; impact resistance; sustainability

check for updates

Citation: Huseien, G.F.; Kubba, Z.; Mhaya, A.M.; Malik, N.H.; Mirza, J. Impact Resistance Enhancement of Sustainable Geopolymer Composites Using High Volume Tile Ceramic Wastes. *J. Compos. Sci.* **2023**, *7*, 73. https://doi.org/10.3390/jcs7020073

Academic Editor: Francesco Tornabene

Received: 8 December 2022
Revised: 9 January 2023
Accepted: 3 February 2023
Published: 9 February 2023

1. Introduction

The construction industry has relied heavily on Ordinary Portland Cement (OPC) as a concrete binder since ancient times [1,2]. Despite widespread agreement that OPC production causes serious environmental damage because it releases substantial amounts of greenhouse gases, no viable substitute has been developed [3]. OPC production is responsible for 6 to 7 percent of global CO_2 emissions [4,5]. Geopolymers, which have only been available for a short time, have recently been introduced as an alternative to traditional concrete in the building industry [6–8]. Geopolymers are better than other building materials [9,10] because they have many good qualities, such as their low cost of production, which comes from recycling a lot of industrial waste, their ability to reduce pollution, their long service lives, their low energy use, their high early strength, and their low risk of catching fire [11–13].

The research shows that the proposed geopolymer concrete (GPC) structural components are just as strong as those made from traditional reinforced concrete. However, similar brittle behaviors to those of concrete, a quasi-brittle material, were seen in GPC during these studies, including main-crack failure modes. Geopolymer paste and GPC are more brittle than similarly strengthened cement paste and concrete, according to research by Pan et al. [14]. The inherent brittleness of GPC would impair the durability of reinforced GPC structural components since water and chloride ions may pass through these fractures. Overly stiff or very low-ductility concretes are generally not considered appropriate for use in the construction industry anywhere in the world. There are several factors that go into making concrete, but one of the most crucial is increasing its ductility [15]. Since it allows stress dispersion and provides an early warning of impending failure [16], ductility is an advantageous structural property of concrete. So, with its ductility improved, concrete is better able to withstand dynamic stresses. Highway pavements, bridge decks, industrial floors, etc., all need concrete with a high capacity for energy absorption and IR. Several supplementary ingredients are used to improve the strength qualities of concrete and make it suitable for the intended use [17,18].

Global tiling production rose by around 5.2 percent between 2008 and 2018, from 8.6 million m^2 to 13.5 million m^2 [19]. From 5 to 7 percent of the ceramic industry's total production is lost due to technical difficulties, according to Medina et al. [20,21]. However, these waste products have a high durability rating and are resistant to biological, chemical, and physical forces of deterioration [22]. Consequently, finding a way to reduce or eliminate the need for landfill disposal is a top priority for the ceramics industry [23]. Ceramic material has been shown to be very resistant to the forces of biological deterioration in several scientific tests [1,24]. Ceramic, due to its crystalline mineral content, has turned out to be an effective cementing additive [25,26] for strengthening concrete's mechanical properties. However, despite its potential new use, only a small fraction of that material finds its way into construction [27]. Its immediate implementation in other fields, then, would seem to be crucial. The building industry's continued reliance on ceramic waste as a raw material guarantees it a vital role in mitigating a wide range of environmental problems, as without requiring major adjustments to their production or application processes, the geopolymer industries may employ ceramic waste. Ceramic waste can be recycled rather than dumped in landfills, saving energy, and protecting the environment. Numerous studies have shown that if most industrial waste was correctly recycled into OPC or OPC-free concrete, the construction sector may be more sustainable and effective [28,29].

Evidence from the past shows that engineered geopolymer composites (EGCs) might be a useful impact-resistant material in protective constructions. EGCs are markedly lighter and have specific environmental benefits over conventional construction materials such as steel fibre-reinforced concrete [30,31] and ultra-high-performance concrete [32,33]. Since the ambient temperature in many parts of Europe, Asia, and the United States may fall below 20 degrees Celsius in the winter, additional investigation into the impact resistance of EGCs at freezing temperatures is necessary before its utilization.

Many studies have looked at how well concrete works using recycled materials such as supplementary cementing chemicals [34] and waste aggregates [35]. However, further study using full-scale models is required to analyse the load-deformation response of components, including recycled aggregates, before they may be used in structural applications. Full-size rectangular reinforced concrete beams, measuring 300 mm by 460 mm by 3000 mm in length, were tested by Arezoumandi et al. [36,37]. They found that beams made with recycled concrete aggregate overlays had the same flexural capacity as control beams but a lower cracking moment.

To reduce carbon dioxide emissions, scientists are looking at geopolymer materials as a long-term replacement for OPC. However, large-scale manufacture and market introduction are being hampered by issues related to mix design and the high molarity of alkaline solutions. This research looks at how GBFS and FA, two TCWs found in high concentrations in tertiary blended geopolymer materials, affect compressive strength and impact resistance, two attributes associated with ductility. The resistance of geopolymers to GBFS and FA replaced by TCWs and activated by low concentration alkaline solutions has been thoroughly investigated. There is potential for expanding the use of geopolymer production processes that rely on ambient heat curing. Thus, this study aims to produce cost-effective, energy-efficient, and carbon dioxide (CO_2)-free geopolymer mortar (GPMs) compositions that perform well under severe circumstances. Several factors were examined in this study.

2. Materials and Methods

2.1. Materials Characterization

For this study, we gathered ceramic tile waste, which is one kind of ceramic industrial waste. The TCWs that were gathered were all the same thickness and had no crystalline coating. They were first put through a jaw crusher, which reduced their size, and then a 600 µm screen, which removed any remaining debris. For six hours, a Los Angeles abrasion machine equipped with 20 stainless steel balls of 40 mm diameter was used to treat the ceramic waste particles that had passed through a 600 µm filter. The steps required to obtain TCWs are shown in Figure 1. The experiment relied on the use of unprocessed, unadulterated GBFS that were sourced from Ipoh, Malaysia. Low calcium fly ash (FA) from the Tanjung Bin power station in Johor, Malaysia, was used to make GPMs. FA is an aluminosilicate resource. TCWs had a light grey colour, GBFS was somewhat off-white, and FA was completely transparent. Their external features are shown in Table 1. FA's specific gravity was less than that of both TCWs (2.6) and GBFS (2.9). The median particle size of TCWs, GBFS, and FA was 35 µm, 12.8 µm, and 10 µm, respectively.

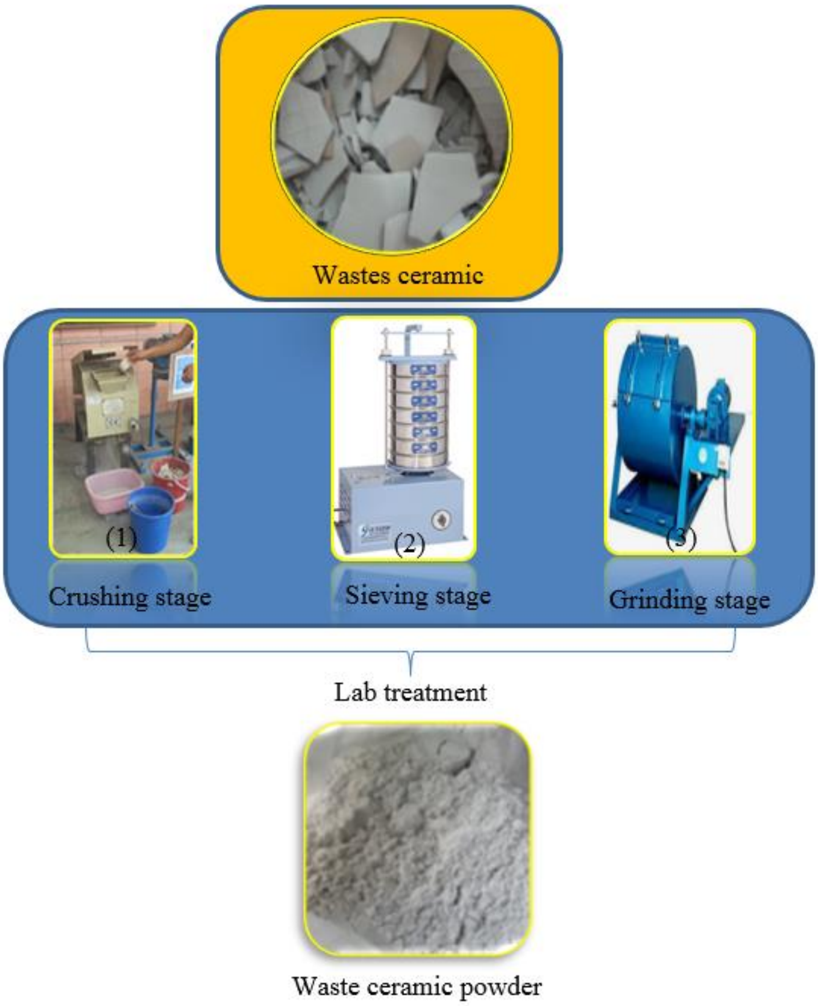

Figure 1. TCWs preparation stages.

Table 1. Chemical and physical attributes of raw materials based on XRF test.

Material Chemical Composition			
Main oxides	TCWs	FA	GBFS
SiO_2	72.6	57.20	30.8
Al_2O_3	12.2	28.81	10.9
CaO	0.02	5.16	51.8
Na_2O	13.46	0.07	0.46
Total	98.28	91.24	93.96
SiO_2:Al_2O_3	5.95	1.98	2.82
CaO:SiO_2	<0.01	0.09	1.68
CaO:Al_2O_3	<0.01	0.18	4.75
NaO:SiO_2	0.18	<0.01	0.01
NaO:Al_2O_3	1.10	<0.01	0.04
Other oxides			
MgO	0.99	1.48	4.57
K_2O	0.03	0.94	0.36
Fe_2O_3	0.56	3.67	0.64
SO_3	0.01	0.10	0.06
LOI	0.13	0.12	0.22
Materials' physical traits			
Specific gravity	2.61	2.2	2.9
Surface area-BET (m^2/g)	12.2	18.1	13.6

The molecular make-up of TCWs, GBFS, and FA was established with the use of X-ray fluorescence spectroscopy (XRF) (Table 1). It proves that the chemical composition of the TCWs, GBFS, and FA determines their unique characteristics. The major components of TCWs, FA, and GBFS were found to be SiO_2 (72.6 percent and 57.8 percent, respectively) and CaO (51.8 percent of GBFS). When compared to the high CaO concentration of GBFS, both TCWs and FA contained negligible amounts (0.02 and 5.2 percent, respectively). When comparing FA, TCWs, and GBFS, Al_2O_3 concentrations were 12.6 percent and 10.9 percent, respectively, with FA having the highest concentration at 28.8 percent. It is generally known that the oxides SiO_2, Al_2O_3, and CaO play crucial roles in the hydration process, leading to the formation of C-(A)-S-H gels. TCW's low Al_2O_3 and CaO concentrations necessitate the addition of materials with high amounts of these elements in order to generate high-performance alkali-activated materials. These materials include FA and GBFS. Mortar strength and density are improved by the addition of GBFS, which provides more calcium, and FA, which adds more aluminium, both of which affect the pozzolanic process to produce more calcium (aluminium) silicate hydrate gels. Because their combined proportion of SiO_2 + Al_2O_3 + Fe_3O_4 is greater than 70 percent, ASTM C618-15 categorises TCWs and FA as class F pozzolans.

The X-ray diffraction (XRD) patterns of TCWs, GBFS, and FA are shown in Figure 2. It has been shown that quartz (SiO_2) and mullite (3 Al_2O_3.2 SiO_2) are the primary crystalline components of TCWs and FA, respectively. By using an internal standard (corundum) and performing an analysis based on the Rietveld method, the amorphous content was determined (shown by the big hump in the background of the XRD pattern centred at 20–30°). It was shown via prior research [38–40], that the FA's responsiveness grows in tandem with its amorphous content. Taking into consideration its 29–40° halo, it seems that GBFS is mostly composed of the amorphous phase with just a small amount of magnetite. The findings of this study agree with those of Ismail et al. [41]. SEM pictures of TCWs, GBFS, and FA are shown in Figure 3. The particles of TCWs were clearly irregular and angular. The GBFS also included angular and irregular particles. Clearly, FA is made up of round, smooth-surfaced particles.

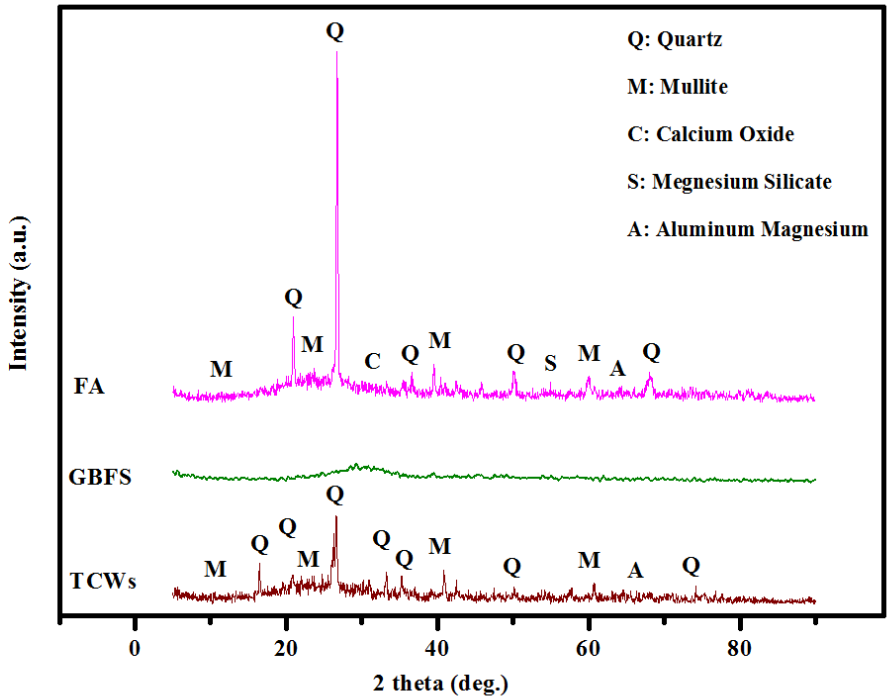

Figure 2. XRD patterns of raw materials included TCWs, GBFS and FA.

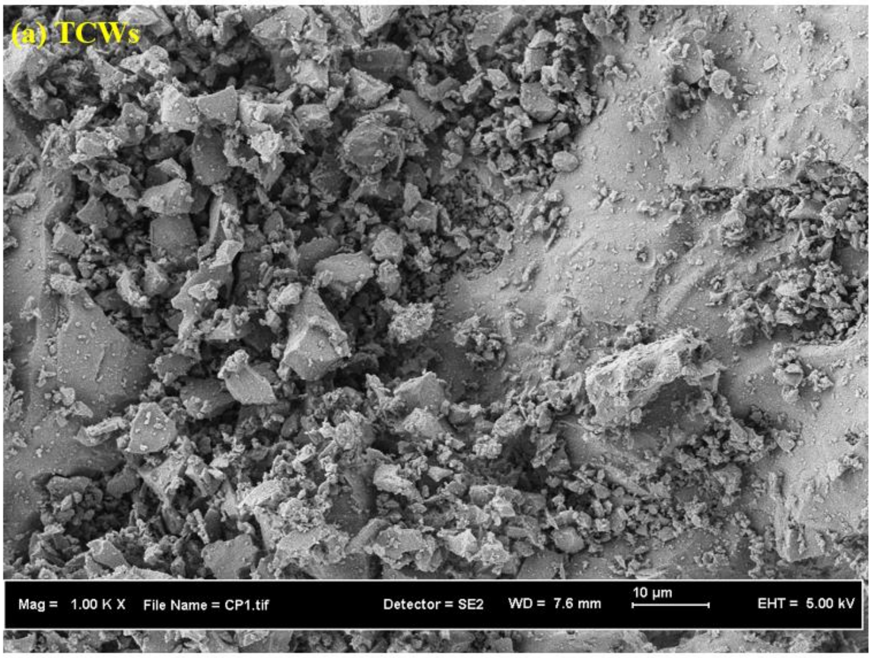

Figure 3. *Cont.*

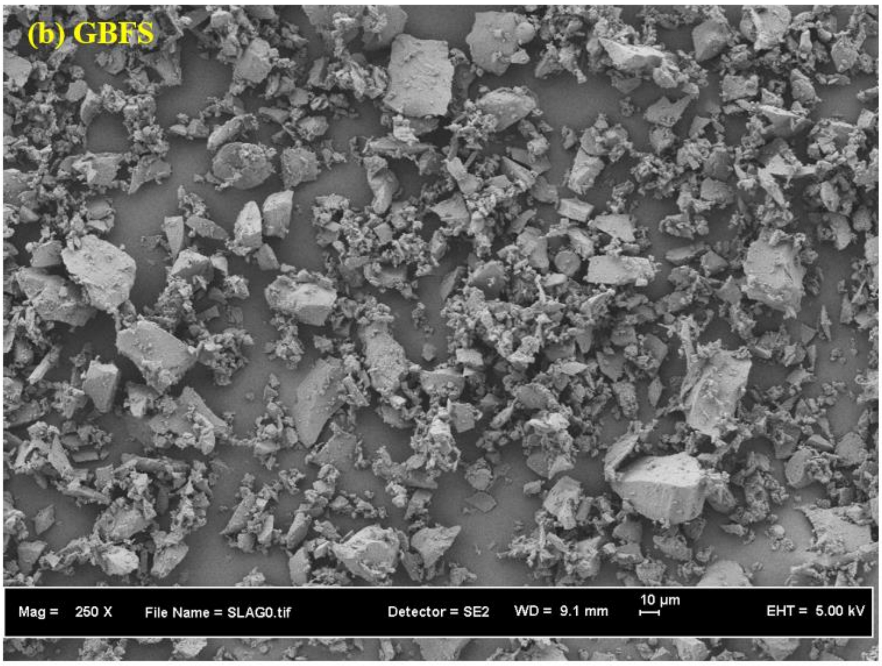

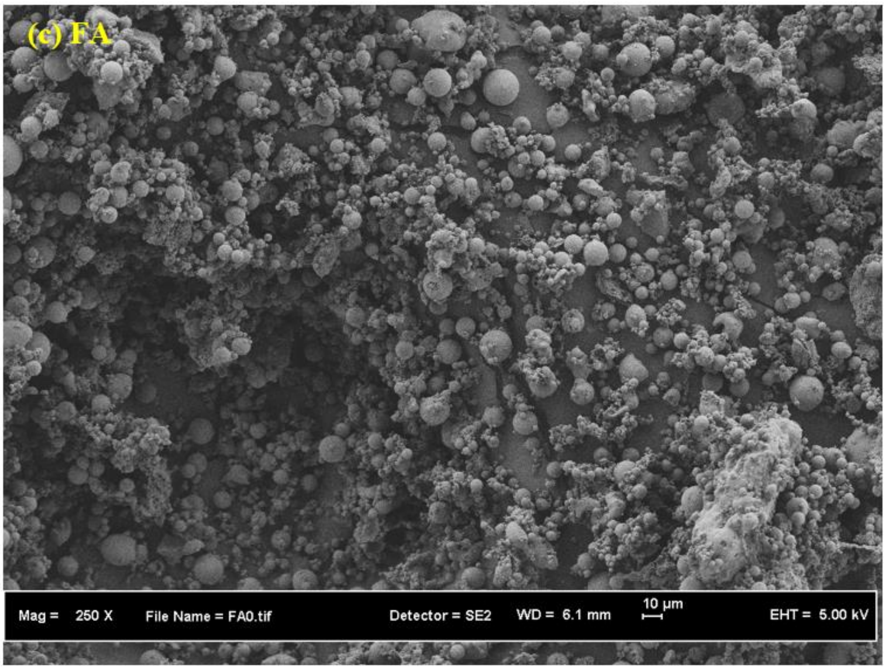

Figure 3. Scanning electronic microscopy (SEM) images of (**a**) TCWs, (**b**) GBFS and (**c**) FA.

Purified sodium hydroxide (NH) pellets and a sodium silicate solution (NS) with the chemical formula SiO_2 (29.5 wt. percent), Na_2O (14.70 wt. percent), and H_2O were utilised in this study (55.80 wt. percent). Using the pellets, we were able to create a 4 M NH solution by dissolving them in water (Figure 4). After being refrigerated for 24 h, this was mixed with NS solution to create a 1.02 SiO_2:Na_2O alkaline solution (S). All alkaline solutions kept the NS:NH ratio below 0.75 to reduce the detrimental environmental effect of sodium silicate (Na_2SiO_3). Sand from local rivers was used for the sieve analysis, as per ASTM C33-16. All the substance passed a 2.36 mm sieve with a specific gravity of 2.6 at a bulk density of 1614 kg/m^3. In this case, a fineness modulus of 2.8 was used.

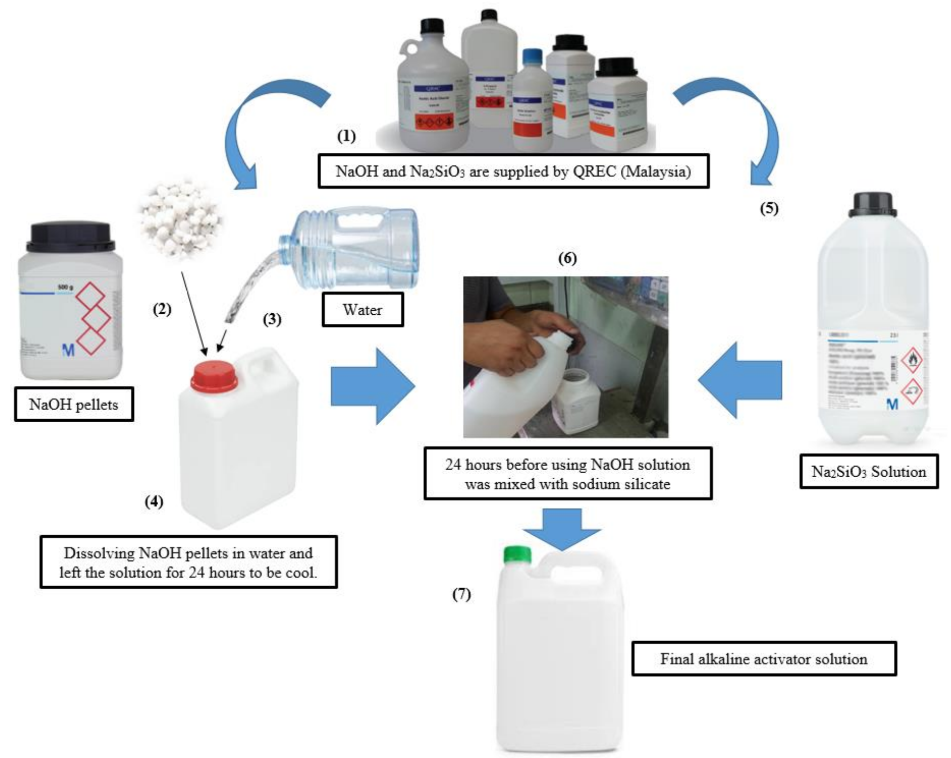

Figure 4. Stages of preparation of two-part alkaline activator solution.

2.2. Mix Design

Alkali-activated mortars with a high percentage of TCWs were tested for their endurance by preparing ten mixes using FA in place of GBFS (Table 2). Each batch contained the same molarity of NH (4 M) and the various percentage of TCWs binder (0, 50, 60 and 70 percent) to ensure uniformity. The ratios of binder to fine aggregate in each mixture were also identical (1.0), as were the ratios of alkaline solution to binder (0.40) and sodium silicate to sodium hydroxide (0.75). The batch with 0 percent TCWs was chosen as the control, and then 50 percent, 60 percent, and 70 percent (by mass ratio) of GBFS were replaced with GBFS in subsequent combinations. The TCWs percentage was held steady at between 50 and 70 percent by weight, the GBFS percentage was held steady at between 20 and 50 percent, and the FA percentage was kept steady at between 0 and 30 percent. The purpose of this set of studies was to determine the impact of a high concentration of ceramic wastes on geopolymer mortar; hence, a wide variety of ternary mixes were tested. All factors were maintained constant except for the percentages of TCWs, GBFS, and FA. Prior to use, NH and NS were mixed in a weighed solution and cooled to room temperature. Before adding the FA, GBFS, and TCWs to the mortar mixer machine to make the GPMs, the fine aggregates were added. Before adding the alkaline solution, they were mixed for two minutes under dry conditions to ensure consistency. After an extra four minutes of mixing, the final liquid was poured into the moulds in accordance with ASTM C579-18. The liquid was poured into the moulds in two stages, with 15 seconds' worth of vibration table time in between each pour to let any trapped air escape. The GPM samples were cured for 24 h at 27 ± 1.5 °C, and 75 percent relative humidity to simulate conditions in Malaysia. In the next step, the specimens were unsealed and kept in the same conditions up until the day of the test.

Table 2. High volume TCWs geopolymer mix design.

Mix		TCWs:GBFS:FA	Binder, kg/m^3			River Sand kg/m^3	Alkaline Solution, kg/m^3	
			TCWs	GBFS	FA		NH	NS
Control	$GPMs_1$	0:50:50	0	550	550	1100	251.24	188.76
Group A	$GPMs_2$	50:50:0	550	550	0	1100	251.24	188.76
	$GPMs_3$	50:40:10		440	110			
	$GPMs_4$	50:30:20		330	220			
	$GPMs_5$	50:20:30		220	330			
Group B	$GPMs_6$	60:40:0	660	440	0	1100	251.24	188.76
	$GPMs_7$	60:30:10		330	110			
	$GPMs_8$	60:20:20		220	220			
Group C	$GPMs_9$	70:30:0	770	330	0	1100	251.24	188.76
	$GPMs_{10}$	70:20:10		220	110			

2.3. Test Procedure

Moulds were cast to ASTM C579's 50 × 50 × 50 mm cube size for more rigorous testing, such as compressive strength. To conduct the flexural strength test, 40 × 40 × 160 mm prisms were cut and stacked. Cylinders with dimensions of 75 mm in diameter and 150 mm in depth were manufactured for tensile strength test. It was decided to use 100 mm in diameter cylinder and 50 mm disk to prepare the samples for the impact resistance test. Oil from an engine was injected into the moulds before casting to make demoulding easier.

The compressive strength test was carried out with ASTM C109 as the standard. At each of the following four ages (1, 3, 7, and 28 days), a minimum of three specimens were tested to determine the compressive strength of the material. ASTM C496, ASTM C78, ASTM C469, and ASTM C140 standards were used to assess the splitting tensile strength, flexural strength, impact resistance, and water absorption, respectively. The analytical technique known as FTIR spectroscopy may be used to differentiate between organic and inorganic compounds. The underlying chemical structures of GPMs were analysed using an FTIR spectrophotometer in order to identify the vibration modes of those structures. The FTIR spectra were collected at room temperature, and the wavenumber range covered 400 cm^{-1} all the way up to 4000 cm^{-1}. In order to investigate the surface morphology of GPMs, scanning electron microscopy (SEM) was used, and the magnification level was optimised. A SEM examination was carried out in order to illustrate the microstructure and diverse degrees of reactivity at various chemical compositions and combinations. To increase the electrical conductivity of the fragments, samples were taken from specimens that were examined at 28 days of age. These samples were then sputtered and coated with gold for two minutes using a machine called a BAL-TEC SCD 005 sputter coater. Finally, the fragments were tested for SEM and FTIR.

The drop-weight test was used for the purposes of measuring the impact resistance of GPMs as well as their capacity to absorb energy during a collision. In line with the recommendations of ACI Committee 544, three cylindrical specimens measuring 100 mm in diameter and 50 mm in height were tested after 28 days for each mix design. As shown in Figure 5, the impact resistance test consisted of repeatedly subjecting the specimen to impact loads (a hammer ball with a diameter of 64 mm and a weight of 4.5 kg), which were delivered from a height of 457 mm. It was then ascertained how many blows were necessary to provide the requisite amount of damage (occurrence of the first crack and failure cracks). The specimen underwent a series of strikes from the hammer ball, and the number of blows (N1) that resulted in the first visible fracture was counted. The number of blows (N2) that caused the opening of cracks at the point at which the concrete components started to crush was also recorded and labelled as the point of ultimate failure. This was the point at which the structure had completely failed.

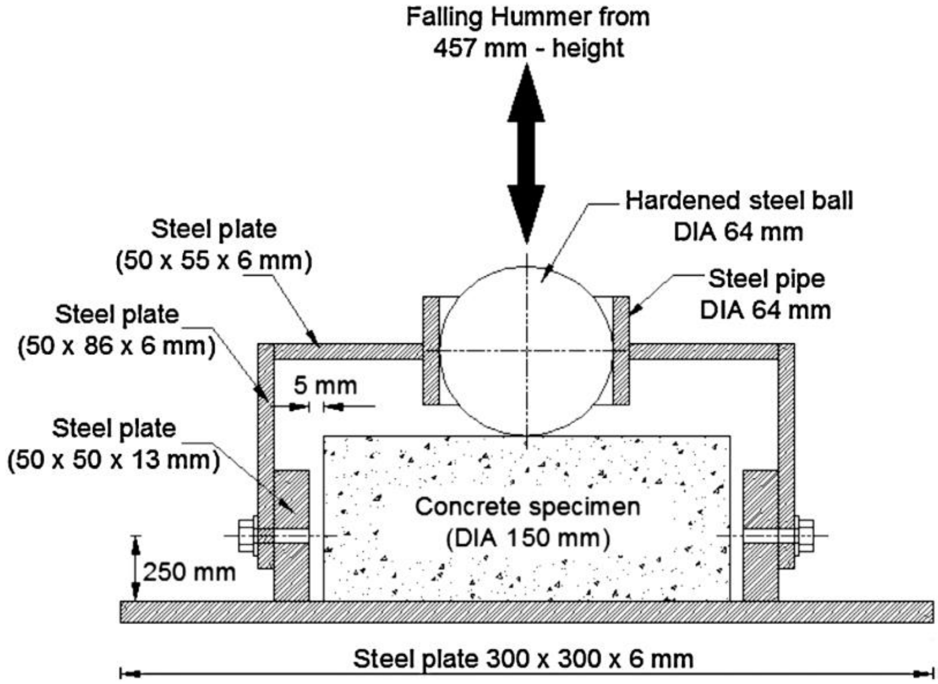

Figure 5. Test rig for impact energy measurement [15].

The following equation calculated the impact energy at the initial crack, Ui (where the subscript i denotes the type of energy absorbed, initial failure):

$$U_i = N_1 mgh \tag{1}$$

Similarly, the impact energy at the ultimate crack, U_u was calculated by the following equation:

$$U_u = N_2 mgh \tag{2}$$

where, N_1 and N_2 are the numbers of blows at the initial and ultimate crack stage, m is the mass of the hammer (4.5 kg), g is gravity acceleration (9.81 m/s^2), and h is the releasing height of the drop hammer (457 mm).

3. Results

3.1. Compressive Strength

Figure 6 depicts the evolution of GPMs compressive strength as a function of high volume TCWs concentration. For all GPMs mixtures, it was found that the compressive strength trend to increase with increasing curing age from 1 to 3 to 7 to 28 days. Compared to the control sample, the compressive strength trend was to decrease with increasing level of replacement GBFS by TCWs and FA. As the TCWs concentration grew from 50 percent to 70 percent after 28 days, the compressive strength of the GPMs fell from 70 MPa to 35 MPa. This drop was connected to the unfavourable consequences of having a low calcium content and a high silica concentration [42–44] in the geopolymer matrix. This resulted in fewer C-(A)-S-H gels, which weakened the GPMs, because TCWs has a higher silica content (more than 70 percent) and a larger particle size (35 µm) than GBFS. On account of this, the development of strength in GPM specimens generated with a high TCWs level was negatively impacted. Figure 6 shows how the compressive strength of GPMs is affected when high volumes of TCWs with FA are used in place of GBFS. A rise in FA concentration has resulted in an increase in silica and alkali, which in turn have a deleterious influence on the amount of calcium (Table 1). Consequently, the fall in GBFS concentration from 50 (GPMs1) to 20 percent (GPMs10) after 28 days of age resulted in a decrease in compressive strength from 80 to 25 MPa. After 28 days of hydration, the compressive strength of all GPM mixtures was higher than it had been after just 7 days. This was in comparison to the initial compressive strength. The low calcium content, which played a key role in the weakening of GPMs, was linked to the existence of low amounts of C-(A)-S-H gels. This was determined to be the case because of the low calcium content. Similar results were reported by Rashad [45], who found that an increase in the concentration of FA in a geopolymer matrix resulted in a decrease in the matrix's compressive strength. The decline in compressive strength may be traced back to several different causes. The first factor was the difference in chemical composition that existed between TCWs, GBFS, and FA. This difference had a significant impact on the alkali activation of binders [46]. The second problem was that the reaction rate of TCWs and FA was much slower than that of partially dissolved GBFS. The third component was associated with the reduction in compactness and density of the geopolymer matrix that occurred as a result of an increase in the TCWs and FA content. The fourth factor was connected to the low sodium hydroxide concentration (4 M), and the compressive strength mostly depended on the calcium oxide content to compensate for the low sodium oxide content. This was because the calcium oxide content was higher than the sodium oxide content. Since this was the case, the GPMs were improved by making more C-S-H and C-A-S-H gels in addition to the N-A-S-H gel.

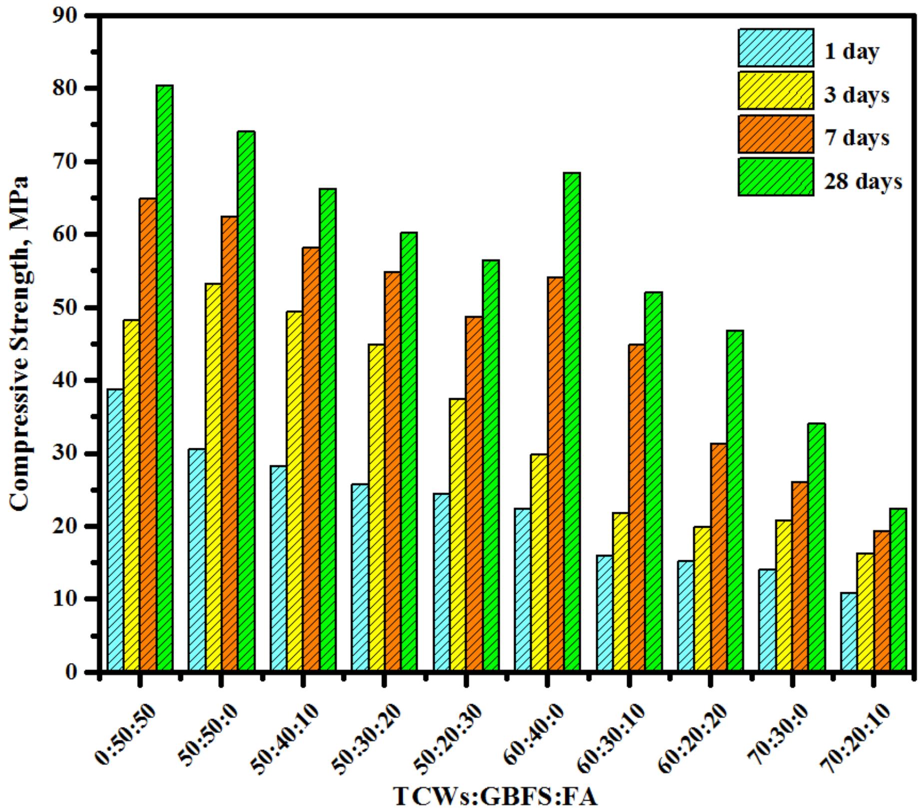

Figure 6. High volume TCWs-content-dependent compressive strength of GPMs.

3.2. Flexural Strength

Figure 7 presents the data that pertains to the flexural strength of GPMs that include a significant quantity of TCWs. At early age (1 day), it was found the flexural strength value dropped from 4.68 MPa to 3.84 MPa with inclusion 50% of TCWs as FA replacement. Likewise, with increasing TCWs content to 60 and 70% as GBFS replacement, the flexural strength trend to decrease to 2.34 and 1.56 MPa, respectively. Likewise, the results of tested specimens after 3 and 7 days show a drop in strength values with increasing TCWs and

FA in geopolymer matrix. At 28 days, we looked at how the TCWs content affected the flexural strength of the material. At 28 days of curing age, the increasing TCWs from 50 percent to 60 and 70 percent significantly effect flexural strength values and led to a drop in the strength from 10.12 MPa to 9.26 and 4.62 MPa, respectively. The effect of FA content, as a GBFS replacement, on the flexural strength of high volume TCWs geopolymer are presented in Figure 7. The power was lessened across the board when the FA concentration in each TCWs level increased. This documented lowest flexural strength of 3.17 MPa was achieved by GPMs10 at 28 days of age, which consisted of 70 percent TCWs and 20 percent GBFS. According to the findings, the flexural strength increased with increasing slag content, which is in line with the findings of previous studies [7,47,48]. It was reported by Van et al. [49] that the addition of more calcined source materials led to increased strength by improving the microstructure of GPMs matrix. Thus, the increase in compressive strength of GPMs specimens by inclusion of GBFS is attributed to the formation of more compact microstructure of the binder [50].

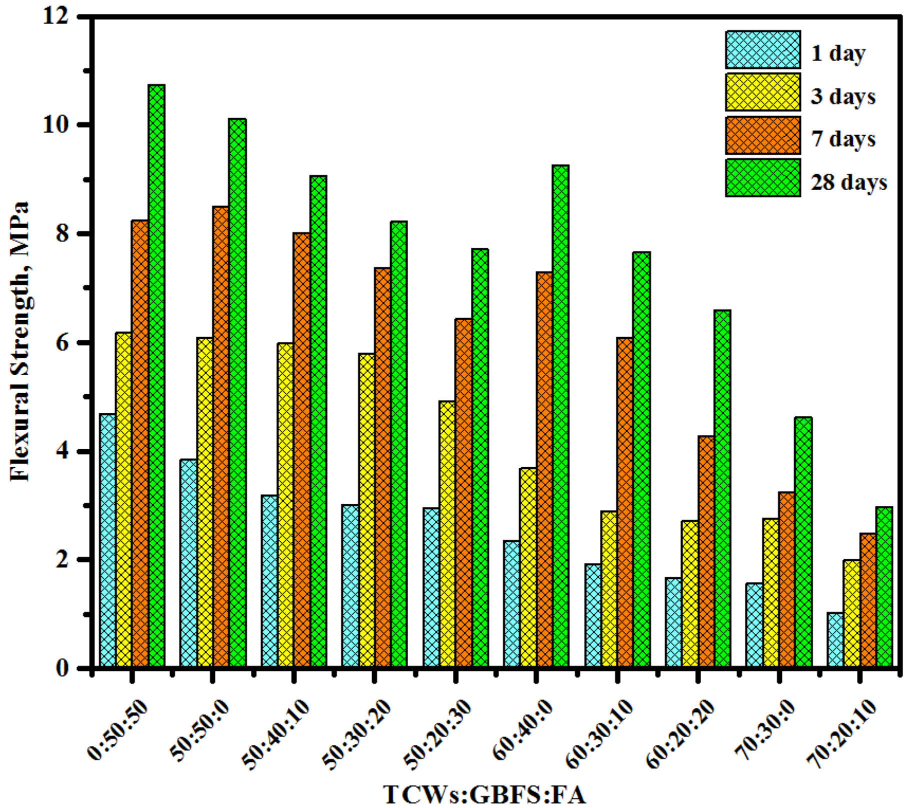

Figure 7. Flexural strength of GPMs for high volume TCWs content at 28 days of age.

3.3. Splitting Tensile Strength

The tensile strength of GPMs that have been loaded with a significant amount of TCWs is shown in Figure 8. When the specimens were 28 days old, measurements were taken to establish their strength values. The tensile strength findings after 28 days were found to be influenced by the rising TCWs concentration. The results showed a lower strength (2.68 MPa) with a high TCWs content (70 percent) in comparison to 5.32 MPa for 50 percent TCWs content and 5.84 MPa for the control sample. The findings also showed that the TCWs content had an influence on the tensile strength findings. At the end of the testing period of 28 days, the findings for splitting tensile strength came in at 5.32 MPa, 5.27 MPa, and 2.68 MPa, respectively, for TCWs concentrations of 50 percent, 60 percent, and 70 percent to replace GBFS. A rise in TCWs caused a calcium concentration drop, which in turn slowed the rate of the chemical reactions needed to produce C-S-H gel [28,42]. Figure 8, with 50, 60, and 70 percent TCWs content, indicate the influence of high volume TCWs on the splitting tensile strength of the GPMs when the FA was replaced by the GBFS.

It was revealed that the amount of FA in GPMs has a link that is opposite to the material's tensile strength. Its potency waned in direct proportion to the increasing supply of FA. The GPMs 10 material had the lowest value of splitting tensile among all the materials in this batch. It included 70 percent TCWs, 20 percent GBFS, and 10 percent FA, and it had a strength of 1.92 MPa after 28 days. Phoo-ngernkham [42] discovered that the additional C–S–H and C–A–S–H gels coexisted with the N–A–S–H gel of fly-ash-based GPMs. This discovery explains the drop in strength that was seen in conjunction with an increase in TCWs and FA content and a decrease in GBFS content.

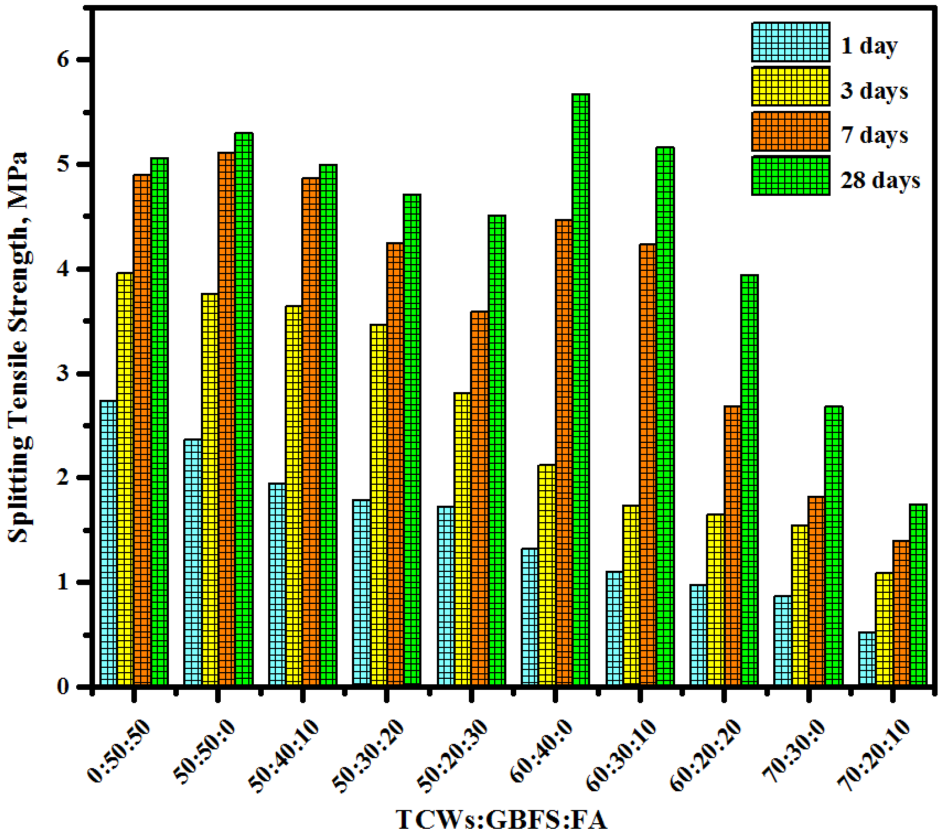

Figure 8. Effect of TCWs content on splitting tensile strength of GPMs at different curing ages.

3.4. Statistical Analysis

The correlations between compressive strength, flexural and splitting tensile strength are presented in Figure 9. In this figure, a direct relationship was found between the compressive strength, flexural strength and splitting tensile strength values. Linear regression methods were applied to correlate the experimental data following Equations (3) and (4), with R^2 values of 0.94 and 0.98 respectively. These values signified high confidence for the relationships. In Figure 10, the statistical results derived from experimental data are presented; and these results indicated that a raise in TCWs and FA content increased the interval difference between the minimum and maximum values of strengths of geopolymer specimens. The frequency histogram of compressive strength of geopolymer specimens is depicted in Figure 10a. These results showed that the compressive strength of specimens was normally distributed and fit well with the superimposed normal distribution curve. For the flexural and splitting tensile strengths, it was found the similar trend to compressive strength and the frequency histogram displayed a normal distribution, as shown in Figure 10b,c, respectively.

$$Y1 = 0.0771\ X \tag{3}$$

$$Y2 = 0.1322\ X \tag{4}$$

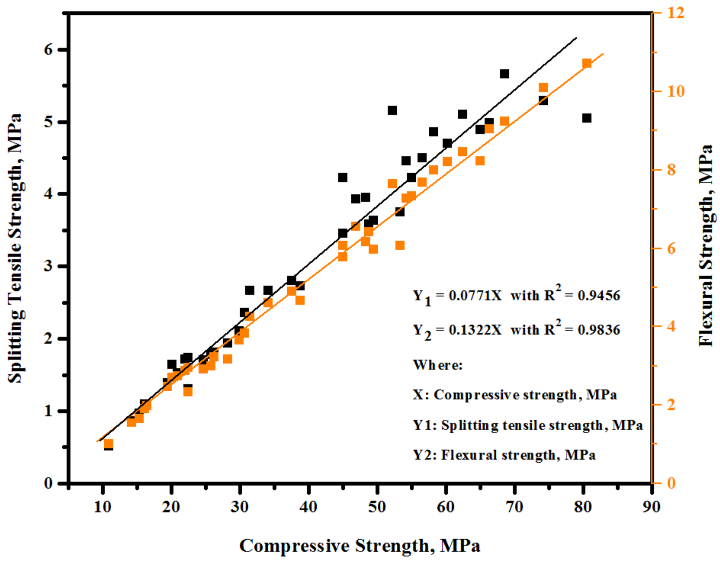

Figure 9. Correlation between compressive strength, flexural and splitting tensile strength of GPMs specimens.

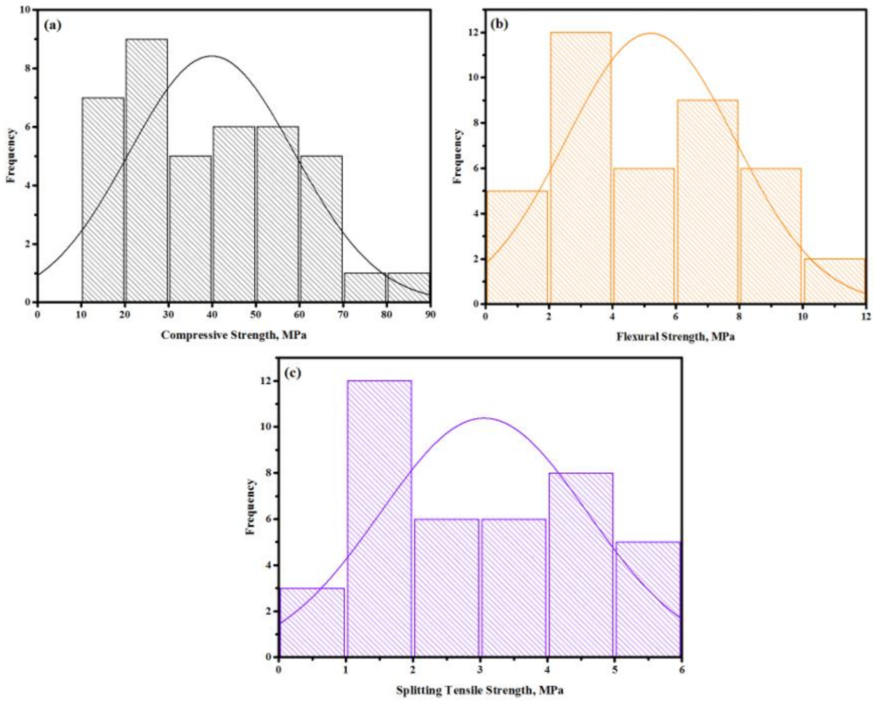

Figure 10. Histograms of strength properties of geopolymers prepared with high volume of TCWs (**a**) compressive strength (**b**) flexural strength (**c**) splitting tensile strength.

3.5. Scanning Electronic Image Analysis

The SEM images of GPMs having a high concentration of TCWs are seen in Figure 11. After 28 days, four specimens were assessed, each of which had either 0, 60, 70 percent TCWs instead of GBFS and 20% FA as GBFS replacement in 60% TCWs matrix. On the surface of the GPMs that were discovered to contain 0 percent TCWs (Figure 12a), there were trace amounts of non-reacted and partially reacted particles. When the TCWs content was increased to 60 and 70 percent, the amount of non-reacted content and partially reacted particles increased (Figure 11b,d, respectively), as compared to the sample that was obtained with 0 percent TCWs (Figure 11a). The rise in TCWs resulted in the production of a morphology with a highly porous structure and a higher quantity of unreacted silica.

This influenced the development of GPM compressive strength, which decreased from 70% MPa to 35 MPa as a result. Figure 11c is a collection of SEM photos that illustrate the impact of replacing 80 percent of the GBFS in synthesised GPMs with by 60% TCWs and 20% FA. These images demonstrate how the surface morphology of the GPMs is altered. Due to the increase in FA concentration from 0 to 20 percent, the surface morphology of the particles has deteriorated, and there is now a greater number of unreacted and partially reacted particles. It has been established that a drop in the concentration of GBFS and an increase in the amount of FA result in a decrease in the C-S-H gel product and the creation of more partially reacted gel, such as mullite, as well as unreacted particles, such as quartz. This change in the C-S-H gel product caused the compressive strength to decrease from 68 MPa to 47 MPa.

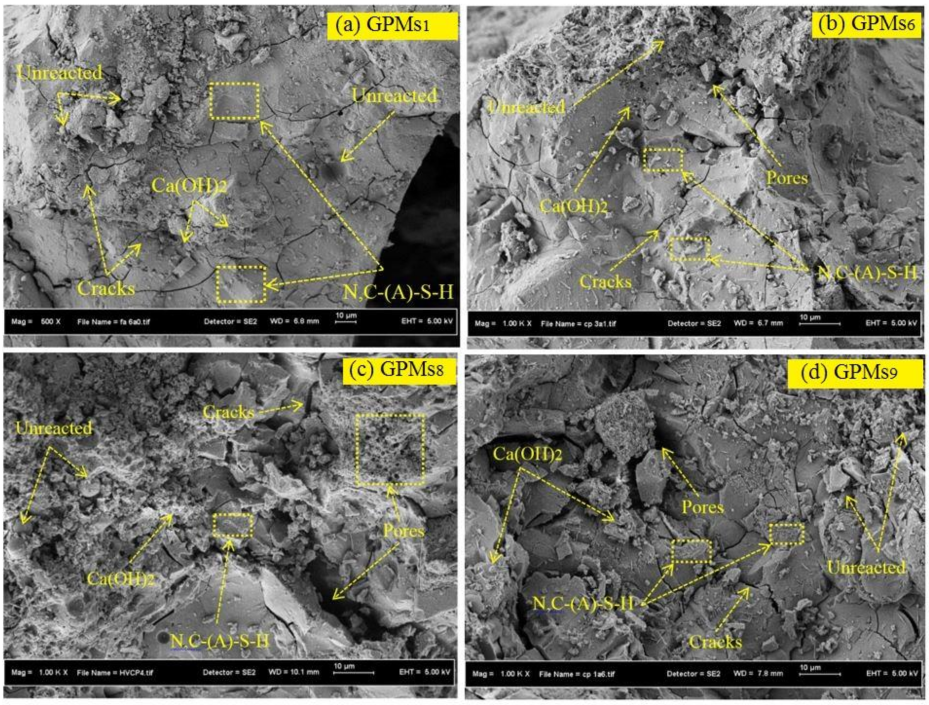

Figure 11. Effect of TCWs and FA as GBFS replacement on the surface morphology of prepared GPMs.

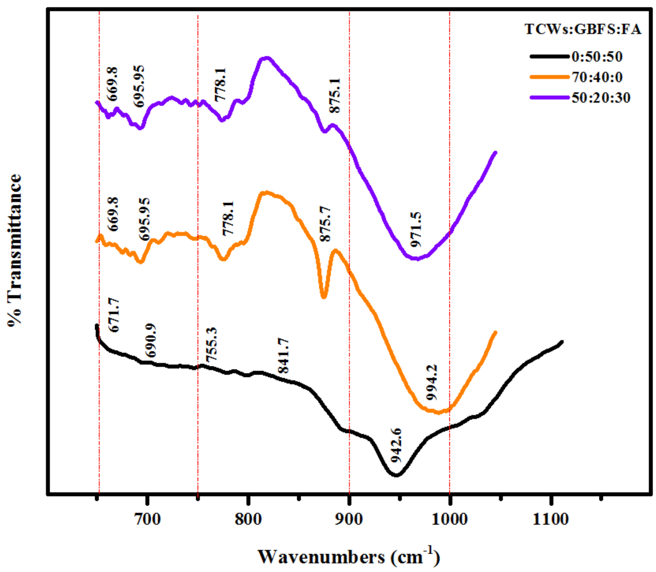

Figure 12. High volume TCWs-GPMs' FTIR spectra in the fingerprint zone.

3.6. FTIR Analysis

According to the findings on compressive strength, a rise in the TCWs content inside the geopolymer matrix as a replacement for GBFS resulted in a significant reduction in the specimens' compressive strength. The progressive decline in strength was caused by the dissolution of CaO and Al_2O_3 as the GBFS level fell [51]. This was the cause of the gradual decrease. It has been discovered that silicate polymerization may be reduced by lowering the total quantity of dissolved aluminium [51–53]. The characterisation of the bonding vibrations in the FTIR spectrum that are responsible for the formation of compressive strength in GPMs is summarised in Figure 12, which can be found here. This hypothesis was proven correct by the appearance of a larger Si–O–Al FTIR spectral band in Figure 13. It was revealed that the band frequency goes up when the TCWs concentration goes up while the GBFS level goes down. When the concentration of TCWs went from 0 percent to 70 percent, respectively, there was a corresponding rise in the frequency of the bands, which went from 942.6 cm^{-1} to 994.2 cm^{-1}. This rise in the frequency of FTIR vibration that was detected might be related to the loss of Al in the GPMs network, which would result in a weaker 3D structure.

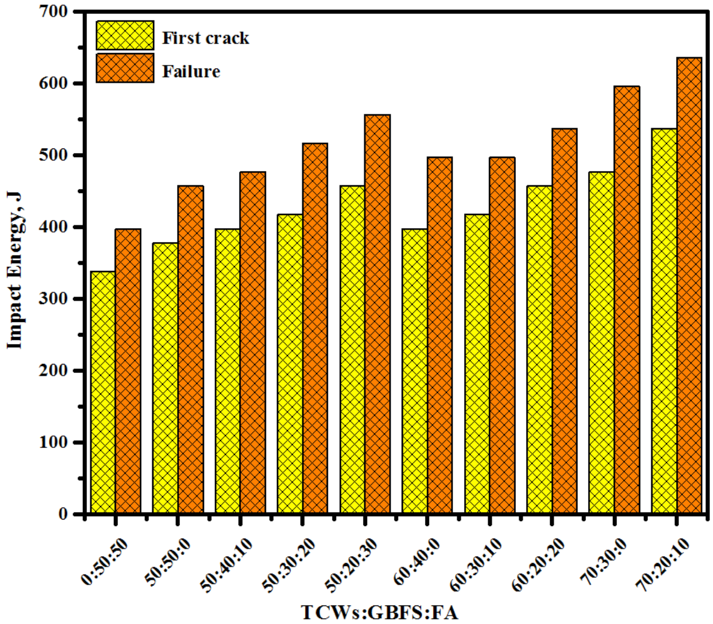

Figure 13. Impact energy of high volume TCWs based geopolymers.

3.7. Evaluation of Impact Energy Capacity

During this experiment, several different concentrations of TCWs were used in order to manufacture GPMs with varying degrees of ductility. The number of blows that were required to generate the first fracture (N1) and failure (N2) of the geopolymer specimen was counted in order to calculate the IR of geopolymers that included 50, 60, or 70 percent TCWs. This was done so that the IR could be calculated. The results of testing performed on geopolymer specimens are shown in Table 3 and include the first fracture, the final crack, the impact energy, and the number of blows required to eventually fail. First, the IR of the samples that were tested was improved by replacing a portion of the GBFS with TCWs (50 percent). The inclusion of TCWs resulted in an increase of 11.7 percent and 14.9 percent, respectively, in the IR measured at the first and final cracks. As the percentage of binders that were replaced with TCWs went up, the IR of initial and final cracking went up for all the samples that were made with TCWs.

Table 3. Impact resistance of all studied geopolymer specimens at the age of 28 days.

Mix	Impact Resistance		N_2-N_1	Impact Energy (J)		PINPB (Blows)
	First Crack (N_1)	Failure (N_2)		First Crack	Failure	
$GPMs_1$	17	20	3	337.71	397.31	17.65
$GPMs_2$	19	23	4	377.44	456.89	21.05
$GPMs_3$	20	24	4	397.31	476.76	20
$GPMs_4$	21	26	5	417.17	516.49	23.81
$GPMs_5$	23	28	5	456.89	556.22	21.74
$GPMs_6$	20	25	5	397.31	496.63	25
$GPMs_7$	21	25	4	417.17	496.63	19.05
$GPMs_8$	23	27	4	456.89	536.36	17.39
$GPMs_9$	24	30	6	476.76	595.95	25
$GPMs_{10}$	27	32	5	536.36	635.68	18.52

Table 3 illustrates how the presence of TCWs acts as a substitute for fine particles and how this affects the IR of geopolymer specimens. The resistance of the specimens to early cracks and failure was increased by 46.8 percent and 49.9 percent, respectively, by increasing the content of fine TCWs from 50 percent to 70 percent. The percentage of TCWs in the material rose from 50 percent to 70 percent and GBFS was replaced by 10 percent of FA, which resulted in an increase in early cracking and failure of 57 percent and 60 percent, respectively. Based on the results presented in Figure 13, the GBFS could be replaced with a mix of TCWs and FA to make the surface as impact resistant as possible.

The value of N2-N1 in Figure 14 for changed geopolymer design mixes demonstrates the effect of varying TCWs concentrations on the post-peak resistance (PPR) of geopolymer. This effect can be seen when the design mixes are altered. When compared to the sample used as a control, the incorporation of TCWs into the concrete mixes that were recommended resulted in a significant increase in the PPR of the specimens that were tested. When compared to the control sample and the other geopolymer specimens, the geopolymer with the highest PPR was the one that had 70% of TCWs as a binder.

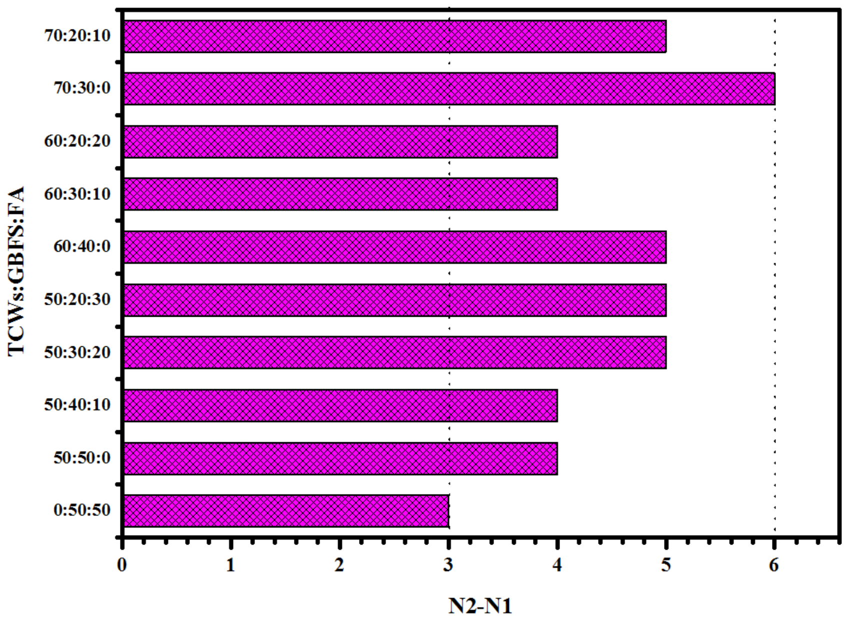

Figure 14. Variation of IR (N_2-N_1) as a function of DRTCs content.

Figure 15 depicts the relationship between the level of TCWs included, and the impact energy capacity at the failure crack. In this diagram, direct correlation was observed between the TCWs content and failure impact energy; as the content of TCWs increased, the impact resistance of geopolymer specimens significantly enhanced. As presented in Equation (5), the linear regression method was applied to correlate the experimental data of geopolymer specimens, with R^2 value of 0.62. This signified good confidence for the relationships.

$$Y = 2.7342\ X + 374.31 \tag{5}$$

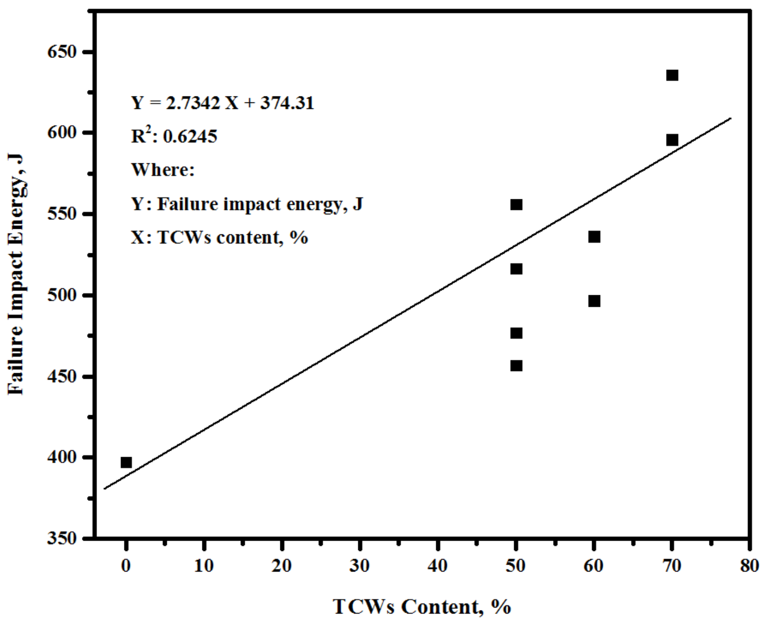

Figure 15. Relationship between TCWs content and impact energy capacity at failure stage.

Figure 16 presents an illustration of the failure processes that might occur in geopolymer specimens that have been generated with significant amounts of TCWs. The findings suggest that specimens with a high concentration of TCWs exhibited scant cracking due to the bridging effect of the TCWs, which gathered more energy and prevented the precipitous collapse of the specimens. The impact energy was absorbed by TCWs rather than being transferred to the surrounding GBFS, which resulted in a significant increase in the IR capacity and a delay in the onset and propagation of cracks in the mortar. This was achieved by delaying the onset of cracking in the mortar. When rubber particles are added to reinforced structures, the impact resistance of those structures goes up substantially when those structures are subjected to both impact and dynamic stresses.

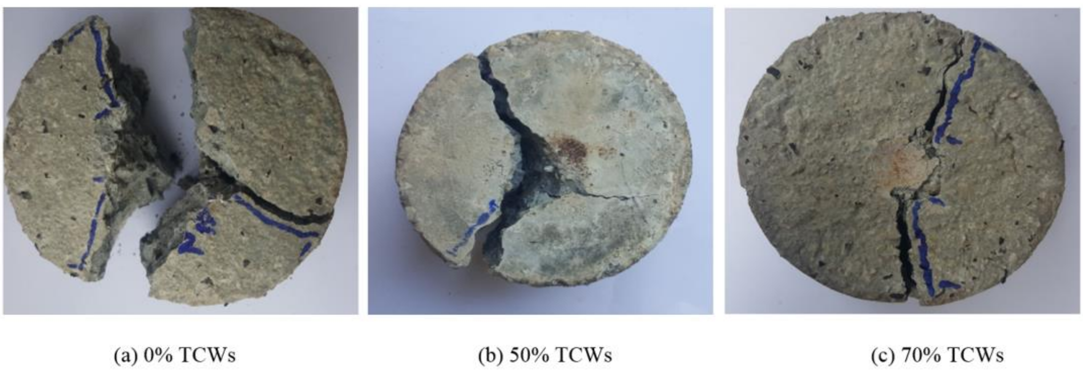

Figure 16. Fracture pattern of high TCWs-based GPMs.

4. Conclusions

The influence of a high concentration of TCWs on the properties of ternary GPMs was investigated, specifically in terms of compressive, flexural and splitting tensile strengths, microstructures, and impact resistance. The following are some of the inferences that may be drawn from the results of the experiment:

The growth of TCW-based GPMs' compressive strength was influenced by the addition of GBFS and FA, which contributed to the material. The strength improvement was diminished when the concentration of GBFS dropped from fifty percent to twenty percent. However, the GPMs that were created by substituting 50 percent TCWs for GBFS achieved a sufficiently high compressive strength of 45.9 MPa, which would allow this product to be used and employed in a variety of applications within the construction sector.

TCWs were used as a partial replacement for GBFS, FA, and this resulted in a marked improvement in the ductility performance by increasing the impact resistance.

On account of the increased TCWs, the improved geopolymer mortar was able to absorb stresses in an effective manner, resulting in a high IR.

The prepared GPMs gave a superior product in terms of mechanical and durability qualities, which is likely to be of interest to many manufacturers of mortar and concrete. In addition to the environmental advantages, these features made the product better. This suggested replacement for traditional cement mortars and concrete has a wide range of applications and has the potential to assist businesses operating in the sustainable construction sector in accomplishing their sustainability objectives.

The effect of high volume TCWs on the drying shrinkage and structural applications of geopolymer concrete need in-depth investigation.

Author Contributions: Conceptualization, G.F.H. and A.M.M.; methodology, G.F.H.; software, Z.K.; validation, G.F.H., Z.K. and J.M.; formal analysis, A.M.M.; investigation, N.H.M.; resources, J.M.; data curation, G.F.H.; writing—original draft preparation, G.F.H.; writing—review and editing, J.M.; visualization, N.H.M.; supervision, J.M.; project administration, Z.K.; funding acquisition, G.F.H. and A.M.M. All authors have read and agreed to the published version of the manuscript.

Funding: This research received no external funding.

Institutional Review Board Statement: Not applicable.

Informed Consent Statement: Not applicable.

Data Availability Statement: Not applicable.

Acknowledgments: The authors thank the National University of Singapore for their support and cooperation to conduct this research.

Conflicts of Interest: The authors declare no conflict of interest.

References

1. Mohammadhosseini, H.; Lim, N.H.A.S.; Tahir, M.M.; Alyousef, R.; Alabduljabbar, H.; Samadi, M. Enhanced performance of green mortar comprising high volume of ceramic waste in aggressive environments. *Constr. Build. Mater.* **2019**, *212*, 607–617.
2. Mhaya, A.M.; Huseien, G.F.; Abidin, A.R.Z.; Ismail, M. Long-term mechanical and durable properties of waste tires rubber crumbs replaced GBFS modified concretes. *Constr. Build. Mater.* **2020**, *256*, 119505. [CrossRef]
3. Samadi, M.; Shah, K.W.; Huseien, G.F.; Lim, N.H.A.S. Influence of glass silica waste nano powder on the mechanical and microstructure properties of alkali-activated mortars. *Nanomaterials* **2020**, *10*, 324. [CrossRef]
4. He, Z.; Zhu, X.; Wang, J.; Mu, M.; Wang, Y. Comparison of CO_2 emissions from OPC and recycled cement production. *Constr. Build. Mater.* **2019**, *211*, 965–973.
5. Singh, N.; Middendorf, B. Geopolymers as an alternative to Portland cement: An overview. *Constr. Build. Mater.* **2020**, *237*, 117455.
6. Barcelo, L.; Kline, J.; Walenta, G.; Gartner, E. Cement and carbon emissions. *Mater. Struct.* **2014**, *47*, 1055–1065. [CrossRef]
7. Huseien, G.F.; Ismail, M.; Tahir, M.M.; Mirza, J.; Khalid, N.H.A.; Asaad, M.A.; Husein, A.A.; Sarbini, N.N. Synergism between palm oil fuel ash and slag: Production of environmental-friendly alkali activated mortars with enhanced properties. *Constr. Build. Mater.* **2018**, *170*, 235–244. [CrossRef]
8. Kubba, Z.; Hewayde, E.; Huseien, G.F.; Sam, A.R.M.; Asaad, M. Effect of sodium silicate content on setting time and mechanical properties of multi blend geopolymer mortars. *J. Eng. Appl. Sci.* **2019**, *14*, 2262–2267.

9. Nawaz, M.; Heitor, A.; Sivakumar, M. Geopolymers in construction-recent developments. *Constr. Build. Mater.* **2020**, *260*, 120472.
10. Kirschner, A.; Harmuth, H. Investigation of geopolymer binders with respect to their application for building materials. *Ceramics-Silikaty* **2004**, *48*, 117–120.
11. Singh, N.B. Fly ash-based geopolymer binder: A future construction material. *Minerals* **2018**, *8*, 299. [CrossRef]
12. Huseien, G.F.; Mirza, J.; Ismail, M.; Ghoshal, S.; Hussein, A.A. Geopolymer mortars as sustainable repair material: A comprehensive review. *Renew. Sustain. Energy Rev.* **2017**, *80*, 54–74. [CrossRef]
13. Huseien, G.F.; Tahir, M.M.; Mirza, J.; Ismail, M.; Shah, K.W.; Asaad, M.A. Effects of POFA replaced with FA on durability properties of GBFS included alkali activated mortars. *Constr. Build. Mater.* **2018**, *175*, 174–186.
14. Pan, Z.; Sanjayan, J.G.; Rangan, B.V. Fracture properties of geopolymer paste and concrete. *Mag. Concr. Res.* **2011**, *63*, 763–771. [CrossRef]
15. Mhaya, A.M.; Huseien, G.F.; Faridmehr, I.; Abidin, A.R.Z.; Alyousef, R.; Ismail, M. Evaluating mechanical properties and impact resistance of modified concrete containing ground Blast Furnace slag and discarded rubber tire crumbs. *Constr. Build. Mater.* **2021**, *295*, 123603. [CrossRef]
16. Mohammadhosseini, H.; Tahir, M.M.; Alaskar, A.; Alabduljabbar, H.; Alyousef, R. Enhancement of strength and transport properties of a novel preplaced aggregate fiber reinforced concrete by adding waste polypropylene carpet fibers. *J. Build. Eng.* **2020**, *27*, 101003.
17. Siddika, A.; Al Mamun, M.A.; Alyousef, R.; Mohammadhosseini, H. State-of-the-art-review on rice husk ash: A supplementary cementitious material in concrete. *J. King Saud Univ.-Eng. Sci.* **2021**, *33*, 294–307.
18. Khankhaje, E.; Hussin, M.W.; Mirza, J.; Rafieizonooz, M.; Salim, M.R.; Siong, H.C.; Warid, M.N.M. On blended cement and geopolymer concretes containing palm oil fuel ash. *Mater. Des.* **2016**, *89*, 385–398. [CrossRef]
19. Samadi, M.; Huseien, G.F.; Mohammadhosseini, H.; Lee, H.S.; Lim, N.H.A.S.; Tahir, M.M.; Alyousef, R. Waste ceramic as low cost and eco-friendly materials in the production of sustainable mortars. *J. Clean. Prod.* **2020**, *266*, 121825.
20. Medina, C.; de Rojas, M.I.S.; Frías, M. Freeze-thaw durability of recycled concrete containing ceramic aggregate. *J. Clean. Prod.* **2013**, *40*, 151–160. [CrossRef]
21. Medina, C.; Banfill, P.F.G.; De Rojas, M.S.; Frías, M. Rheological and calorimetric behaviour of cements blended with containing ceramic sanitary ware and construction/demolition waste. *Constr. Build. Mater.* **2013**, *40*, 822–831.
22. Rashid, K.; Razzaq, A.; Ahmad, M.; Rashid, T.; Tariq, S. Experimental and analytical selection of sustainable recycled concrete with ceramic waste aggregate. *Constr. Build. Mater.* **2017**, *154*, 829–840. [CrossRef]
23. Lim, N.H.A.S.; Mohammadhosseini, H.; Tahir, M.M.; Samadi, M.; Sam, A.R.M. Microstructure and strength properties of mortar containing waste ceramic nanoparticles. *Arab. J. Sci. Eng.* **2018**, *43*, 5305–5313.
24. Senthamarai, R.; Manoharan, P.D. Concrete with ceramic waste aggregate. *Cem. Concr. Compos.* **2005**, *27*, 910–913.
25. Siddique, S.; Chaudhary, S.; Shrivastava, S.; Gupta, T. Sustainable utilisation of ceramic waste in concrete: Exposure to adverse conditions. *J. Clean. Prod.* **2019**, *210*, 246–255.
26. Huseien, G.F.; Sam, A.R.M.; Shah, K.W.; Mirza, J.; Tahir, M.M. Evaluation of alkali-activated mortars containing high volume waste ceramic powder and fly ash replacing GBFS. *Constr. Build. Mater.* **2019**, *210*, 78–92.
27. Zimbili, O.; Salim, W.; Ndambuki, M. A review on the usage of ceramic wastes in concrete production. *Int. J. Civ. Environ. Struct. Constr. Archit. Eng.* **2014**, *8*, 91–95.
28. Huseien, G.F.; Sam, A.R.M.; Shah, K.W.; Asaad, M.A.; Tahir, M.M.; Mirza, J. Properties of ceramic tile waste based alkali-activated mortars incorporating GBFS and fly ash. *Constr. Build. Mater.* **2019**, *214*, 355–368.
29. Gautam, L.; Jain, J.K.; Kalla, P.; Choudhary, S. A review on the utilization of ceramic waste in sustainable construction products. *Mater. Today Proc.* **2021**, *43*, 1884–1891.
30. Awal, A.A.; Mohammadhosseini, H. Green concrete production incorporating waste carpet fiber and palm oil fuel ash. *J. Clean. Prod.* **2016**, *137*, 157–166.
31. Abbas, A.-G.N.; Aziz, F.N.A.A.; Abdan, K.; Nasir, N.A.M.; Huseien, G.F. A state-of-the-art review on fibre-reinforced geopolymer composites. *Constr. Build. Mater.* **2022**, *330*, 127187. [CrossRef]
32. Li, J.; Wu, Z.; Shi, C.; Yuan, Q.; Zhang, Z. Durability of ultra-high performance concrete—A review. *Constr. Build. Mater.* **2020**, *255*, 119296.
33. Yoo, D.-Y.; Banthia, N. Mechanical and structural behaviors of ultra-high-performance fiber-reinforced concrete subjected to impact and blast. *Constr. Build. Mater.* **2017**, *149*, 416–431.
34. Thomas, M. The effect of supplementary cementing materials on alkali-silica reaction: A review. *Cem. Concr. Res.* **2011**, *41*, 1224–1231.
35. Gupta, P.K.; Khaudhair, Z.A.; Ahuja, A.K. A new method for proportioning recycled concrete. *Struct. Concr.* **2016**, *17*, 677–687.
36. Arezoumandi, M.; Smith, A.; Volz, J.S.; Khayat, K.H. An experimental study on shear strength of reinforced concrete beams with 100% recycled concrete aggregate. *Constr. Build. Mater.* **2014**, *53*, 612–620. [CrossRef]
37. Arezoumandi, M. Feasibility of crack free reinforced concrete bridge deck from materials composition perspective: A state of the art review. *Front. Struct. Civ. Eng.* **2015**, *9*, 91–103. [CrossRef]
38. Yusuf, M.O.; Johari, M.A.M.; Ahmad, Z.A.; Maslehuddin, M. Evolution of alkaline activated ground blast furnace slag–ultrafine palm oil fuel ash based concrete. *Mater. Des.* **2014**, *55*, 387–393.

39. Temuujin, J.; van Riessen, A.; MacKenzie, K. Preparation and characterisation of fly ash based geopolymer mortars. *Constr. Build. Mater.* **2010**, *24*, 1906–1910.
40. Rickard, W.D.; Williams, R.; Temuujin, J.; Van Riessen, A. Assessing the suitability of three Australian fly ashes as an aluminosilicate source for geopolymers in high temperature applications. *Mater. Sci. Eng. A* **2011**, *528*, 3390–3397.
41. Ismail, I.; Bernal, S.A.; Provis, J.L.; San Nicolas, R.; Hamdan, S.; van Deventer, J.S. Modification of phase evolution in alkali-activated blast furnace slag by the incorporation of fly ash. *Cem. Concr. Compos.* **2014**, *45*, 125–135.
42. Phoo-ngernkham, T.; Sata, V.; Hanjitsuwan, S.; Ridtirud, C.; Hatanaka, S.; Chindaprasirt, P. High calcium fly ash geopolymer mortar containing Portland cement for use as repair material. *Constr. Build. Mater.* **2015**, *98*, 482–488.
43. Nath, P.; Sarker, P.K. Effect of GGBFS on setting, workability and early strength properties of fly ash geopolymer concrete cured in ambient condition. *Constr. Build. Mater.* **2014**, *66*, 163–171.
44. Huseiena, G.F.; Ismaila, M.; Tahirb, M.; Mirzac, J.; Husseina, A.; Khalida, N.H.; Sarbinia, N.N. Effect of binder to fine aggregate content on performance of sustainable alkali activated mortars incorporating solid waste materials. *Chem. Eng.* **2018**, *63*, 667–672.
45. Rashad, A.M. Properties of alkali-activated fly ash concrete blended with slag. *Iran. J. Mater. Sci. Eng.* **2013**, *10*, 57–64.
46. Puertas, F.; Martínez-Ramírez, S.; Alonso, S.; Vázquez, T. Alkali-activated fly ash/slag cements: Strength behaviour and hydration products. *Cem. Concr. Res.* **2000**, *30*, 1625–1632.
47. Song, S.; Jennings, H.M. Pore solution chemistry of alkali-activated ground granulated blast-furnace slag. *Cem. Concr. Res.* **1999**, *29*, 159–170.
48. Al-Majidi, M.H.; Lampropoulos, A.; Cundy, A.; Meikle, S. Development of geopolymer mortar under ambient temperature for in situ applications. *Constr. Build. Mater.* **2016**, *120*, 198–211. [CrossRef]
49. Van Jaarsveld, J.; Van Deventer, J.; Lukey, G. The effect of composition and temperature on the properties of fly ash-and kaolinite-based geopolymers. *Chem. Eng. J.* **2002**, *89*, 63–73. [CrossRef]
50. Deb, P.S.; Nath, P.; Sarker, P.K. The effects of ground granulated blast-furnace slag blending with fly ash and activator content on the workability and strength properties of geopolymer concrete cured at ambient temperature. *Mater. Des.* **2014**, *62*, 32–39.
51. Puligilla, S.; Mondal, P. Role of slag in microstructural development and hardening of fly ash-slag geopolymer. *Cem. Concr. Res.* **2013**, *43*, 70–80.
52. García-Lodeiro, I.; Fernández-Jiménez, A.; Palomo, A.; Macphee, D.E. Effect of calcium additions on N–A–S–H cementitious gels. *J. Am. Ceram. Soc.* **2010**, *93*, 1934–1940.
53. Huseien, G.F.; Faridmehr, I.; Nehdi, M.L.; Abadel, A.A.; Aiken, T.A.; Ghoshal, S. Structure, morphology and compressive strength of Alkali-activated mortars containing waste bottle glass nanoparticles. *Constr. Build. Mater.* **2022**, *342*, 128005. [CrossRef]